LANGMUIR

Interface Components: Nanoparticles, Colloids, Emulsions, Surfactants, Proteins, Polymers

Quaternary Amine-Terminated Quantum Dots Induce Structural Changes to Supported Lipid Bilayers

Arielle C Mensch, Joseph T. Buchman, Christy L. Haynes, Joel A. Pedersen, and Robert J Hamers

Langmuir, **Just Accepted Manuscript** • DOI: 10.1021/acs.langmuir.8b02047 • Publication Date (Web): 05 Sep 2018

Quaternary Amine-Terminated Quantum Dots Induce Structural Changes to Supported Lipid Bilayers

Arielle C. Mensch,[†,⊥] Joseph T. Buchman,[∥] Christy L. Haynes,[∥] Joel A. Pedersen,[†‡§] and Robert J. Hamers[*†]*

[†]Department of Chemistry, University of Wisconsin, Madison, WI 53706, United States

[∥] Department of Chemistry, University of Minnesota, Minneapolis, MN 55455, United States

[‡]Department of Soil Science, University of Wisconsin, Madison, WI 53706, United States

[§]Department of Civil and Environmental Engineering, University of Wisconsin, Madison, WI 53706, United States

ABSTRACT

The cytoplasmic membrane represents an essential barrier between the cytoplasm and the environment external to cells. Interaction with nanomaterials can alter the integrity of the cytoplasmic membrane through the formation of holes and membrane thinning, which can ultimately lead to adverse biological impacts. Here we use supported lipid bilayers as experimental models for the cytoplasmic membrane to investigate the impact of quantum dots functionalized with the cationic polymer

poly(diallyldimethylammonium chloride) (PDDA) on membrane structure. Using quartz crystal microbalance with dissipation monitoring we show that the positively charged quantum dots attach to and induce structural rearrangement to zwitterionic bilayers in solely the liquid-disordered phase and in those containing phase-segregated liquid-ordered domains. Real-time atomic force microscopy imaging revealed that PDDA-coated quantum dots, and to a lesser extent PDDA itself, induced disappearance of liquid-ordered domains. We hypothesize this effect is due to an increase in energy per unit area caused by collisions between PDDA-coated quantum dots at the membrane surface. This increase in free energy per area exceeds the approximate free energy change associated with membrane mixing between the liquid-ordered and liquid-disordered phases and results in the destabilization of membrane domains.

INTRODUCTION

Increasing deployment of nanomaterials in consumer products and commercial processes raises concerns that engineered nanomaterials released into the environment may interact adversely with organisms.[1-3] However, understanding the impact of nanomaterials on organisms at a mechanistic level is difficult and requires a systematic approach using complementary analytical tools.[3-5] Prior studies have indicated a number of different possible modes of interaction occurring at the nano-bio interface, including endocytic uptake,[6-7] passive diffusion, membrane permeabilization,[8-9] lipid extraction,[10] and indirect interactions such as ROS generation[11] or ion dissolution.[12] The potential interactions between nanoparticles and cell surfaces are complex, may occur through a number of different mechanisms, and ultimately depend on the type of nanomaterial and cell surface structure.

For eukaryotic organisms, the initial interaction with nanomaterials frequently involves contact with the cytoplasmic membrane, which can result in internalization and be a first step toward inducing toxic responses.[13-14] Supported lipid bilayers (SLBs) are frequently used as model systems to gain fundamental

insights into nanoparticle-membrane interactions.[15-18] While SLBs do not recapitulate the full complexity of cell membranes, they provide a higher degree of control than can be achieved *in vivo* because their composition can be systematically varied to investigate the influence of biomolecules that are important in the structure and function of cell membranes.[15, 19-20] Prior studies have shown that nanomaterials can induce a number of changes in SLBs including hole formation,[18, 21-22] membrane thinning,[18] and morphological changes.[23]

Cell membranes contain many components that phase segregate into domains exhibiting different degrees of structural order. Laterally organized domains (frequently referred to as membrane rafts or nanodomains) are important features of eukaryotic and prokaryotic membranes[24] and play roles in signal transduction and membrane trafficking.[25] In eukaryotes, sphingolipids and cholesterol often mediate the domain structures in cellular membranes.[26] In lipid bilayers, segregation into liquid-ordered (L_o) and liquid-disordered (L_d) can be induced to study aspects of the phase segregation that occurs in cytoplasmic membranes. Prior work using phase-segregated bilayers showed that the interaction with amphiphilic dendrimers varied depending on the bilayer phase.[27] Partial solubilization occurred with fluid-phase bilayers, while local depressions and flexible lipid patches occurred with gel-phase bilayers, and a ribbon-like network with spherical aggregates occurred with bilayers having both fluid and gel phases.[27] Other studies showed that hydrophilic quantum dots[28] and polycationic dendrimers[29-30] interact preferentially with L_o domains, and that anionic diamond nanoparticles alter the domain shape and packing.[31] In recent work, we showed that 4-nm mercaptopropylamine-capped gold nanoparticles interacted to a larger extent with SLBs containing phase-segregated L_o and L_d domains than with SLBs comprised solely of the L_d phase.[15] These studies suggest that liquid-ordered regions or their boundaries may play an important role in controlling nanoparticle interactions, but a real-time, molecular-level understanding of the interactions remains elusive.

The objective of this study was to use complementary real-time, *in situ* characterization methods to directly observe the impacts of cationic nanoparticles on liquid-ordered domains in supported lipid bilayers. We chose CdSe/ZnS core/shell quantum dots wrapped with a cationic, amphiphilic polymer, poly(diallyldimethylammonium chloride) (PDDA), as a model nanoparticle system. PDDA was chosen because prior studies have shown that cationic nanoparticles interact more strongly with lipid bilayers compared with uncharged or anionic nanoparticles[15, 18, 32-33] and because wrapping with PDDA yielded colloidally stable nanoparticles under the conditions of our experiments. We chose CdSe/ZnS quantum dots because of their technological relevance,[34-35] and thus the concern of environmental release[36] and toxicity.[37] As model bilayers, we studied one composition forming a L_d phase and a second composition containing both L_d and L_o phases through the inclusion of sphingomyelin and cholesterol, two biomolecules enriched in the phase-segregated "rafts" found in eukaryotic cell membranes,[38] into the SLBs. We use real-time, *in situ* atomic force microscopy (AFM) time-lapse imaging to directly observe the influence of the nanoparticles on the size and shape of the phase-segregated regions over time, and quartz crystal microbalance with dissipation monitoring (QCM-D) to assess net changes in mass associated with the interaction. AFM results show that the introduction of PDDA-QDs to phase-segregated bilayers leads to the shrinking of the liquid-ordered regions, eventually leading to complete loss of the L_o regions. Our results suggest that increased energy per area induced by nanoparticle-nanoparticle collisions may alter membrane structure by reducing the molecular driving forces for phase segregation.

EXPERIMENTAL

Quantum Dot Characterization. Cadmium selenide core quantum dots with a zinc sulfide shell and a positively charged poly(diallyldimethylammonium chloride) (PDDA) polymer wrapping (average molecular mass of 200,000 Da) were procured from OceanNanotech (QSQ-620, manufacturer reported

core size 3.3 nm, shell thickness 2.5 nm, and PDDA thickness 2 nm). The polymer wrapping ensured colloidal stability in water and allowed us to probe the impact of a positively charged particle on the lipid bilayers. We measured the diffusivities and electrophoretic mobilities of the PDDA-QDs by dynamic light scattering and laser Doppler microelectrophoresis (Malvern Zetasizer Nano ZS) at a 1 nM number concentration of QDs in 0.010 M NaCl buffered to pH 7.4 with 0.010 M HEPES. The diffusivity and electrophoretic mobility measurements were the average of five measurements. An intensity correlation function was used to determine the diffusion coefficient of the particles. From the diffusion coefficient we determined the hydrodynamic diameter using the Stokes-Einstein equation and from these values estimated number-averaged hydrodynamic diameter (d_h) using Mie theory.[39] Transmission electron microscopy was conducted on a Tecnai T12 microscope to determine the core size of the particles. Additional sample preparation details can be found in the Supporting Information.

Lipid Vesicle Preparation and Characterization. We prepared small unilamellar vesicles composed solely of 1,2-dioleoyl-*sn*-glycero-3-phosphocholine (DOPC, 850375C, Avanti Polar Lipids) or DOPC with plant-derived cholesterol (Chol, 700100P, Avanti Polar Lipids) and sphingomyelin from chicken egg yolk (SM, S0756, Sigma Aldrich) as previously described.[15] The gel-to-liquid crystalline phase transition temperatures for DOPC and 16:0 SM (the bulk component of the egg yolk SM) are –21 °C[40] and 41 °C[41], respectively. Briefly, stock solutions of Chol and SM were dissolved in chloroform (1 mg/mL) and sonicated for 30 min. The three components were mixed to the desired ratio (100% DOPC or 60/20/20 mol% DOPC/SM/Chol), the chloroform was removed under a stream of nitrogen gas, and any residual chloroform was removed under vacuum overnight. The dried film was rehydrated in 0.001 M NaCl buffered to pH 7.4 with 0.01 M HEPES and vortexed briefly followed by sonication for 30 min to leave a cloudy solution. Following three cycles of freezing with liquid nitrogen and thawing by sonication, the solution was extruded 11 times (Avanti 610000 extruder kit) through a 50 nm polycarbonate membrane

filter (Whatman) to give small unilamellar vesicles. Vesicles were stored at 4 °C and used within one week of extrusion.

Quartz Crystal Microbalance with Dissipation Monitoring. Quartz crystal microbalance with dissipation monitoring measures changes in resonance frequency (Δf) and changes in dissipation (Δ*D*) due to the interaction of an analyte (PDDA-QDs in our case) with the surface of an AT-cut quartz crystal oscillating in shear mode parallel to the bilayer. Changes in frequency are related to the mass of the surface-bound analyte and any hydrodynamically coupled water present at the sensor surface. For laterally homogeneous adlayers, changes in the energy dissipation or damping are related to the resulting film's viscoelasticity, whereas for films of discrete nanosized objects, Δ*D* is related to the stiffness of the particle-surface contacts.[42] For rigidly adsorbed films, defined as $-\Delta D_v/(\Delta f_v/v) << 2/(f_v)$ (equal to 4×10^{-7} Hz^{-1} for the 4.96 MHz crystals used here)[42], where *v* is the harmonic number, the adsorbed surface mass density ($\Delta\Gamma_{QCM\text{-}D}$) is linearly proportional to the change in frequency, as described by the Sauerbrey equation:[43]

$$\Delta\Gamma_{\text{QCM-D}} = -\frac{C}{v}\Delta f_v \qquad (1)$$

where *C* is the mass sensitivity constant (equal to 18.0 $ng \cdot Hz^{-1} \cdot cm^{-2}$ for a 4.96 MHz crystal). In all experiments presented, $-\Delta D_v/(\Delta f_v/v) < 4 \times 10^{-7}$ Hz^{-1} and the Sauerbrey equation was applied to estimate the surface mass density when noted.

Prior to use, SiO_2-coated QCM-D crystals (QSX303, Biolin Scientific, Gothenburg, Sweden) were soaked in a 2% sodium dodecyl sulfate solution for 10 min, rinsed three times alternatively with ultrapure water and ethanol, dried with N_2 gas, and exposed to UV/ozone from a low-pressure mercury lamp for 20 min (Bioforce Nanosciences UV/Ozone Procleaner, 185 and 254 nm). The crystals were then

loaded into temperature-controlled, liquid flow cells (QFM 401, Biolin Scientific) on a Q-Sense E4 instrument (Biolin Scientific).

We formed supported lipid bilayers on the SiO_2 sensor from small unilamellar vesicles composed of purely DOPC or 60/20/20 mol% DOPC/SM/Chol using the vesicle fusion method.[15, 44] The sensors were equilibrated in 0.150 M NaCl buffered to pH 7.4 with 0.010 M HEPES (pH and buffer concentration used throughout) and flowed until a stable baseline was reached. A solution of vesicles (0.03125 $mg \cdot mL^{-1}$) in the same solution was flowed (0.100 $mL \cdot min^{-1}$) over the surface until the critical surface vesicle concentration[45] was attained, at which point, the vesicles fused and ruptured to spontaneously form a supported lipid bilayer. Any loosely adsorbed vesicles were rinsed away and a stable baseline was established by rinsing with vesicle-free solution. The ionic strength of the solution was lowered to 0.010 M NaCl until the frequency and dissipation values stabilized.

Suspensions of 1 nM PDDA-QDs in 0.010 M NaCl were vortexed and immediately flowed over the bilayers. Attachment was monitored for 20 min followed by rinsing with nanoparticle-free solution, until stable frequency and dissipation values were observed, to examine the reversibility of the interaction and any other changes induced by rinsing. Control experiments examined the interaction of PDDA-QDs with the underlying SiO_2 sensor. All attachment experiments were carried out at 25.0 ± 0.5 °C in at least triplicate.

Atomic Force Microscopy. We acquired AFM images of supported lipid bilayers before and after exposure to PDDA-QDs. Supported lipid bilayers were formed on atomically flat surfaces of mica. Mica substrates (Highest Grade V1, Ted Pella) were adhered to glass bottom dishes (P60G-1.5-30-F, MatTek Corporation) using 5-minute epoxy (ITW Polymer Adhesives) and then cleaved using double-sided tape to produce clean, atomically flat surfaces. We equilibrated the mica with 3 mL of 0.150 M NaCl and

0.005 M $CaCl_2$ buffered to pH 7.4 with 0.010 M HEPES for at least 20 min. Calcium was used to facilitate the adsorption of the negatively charged vesicles on the negatively charged mica.[46] The mica remained completely submerged during initial equilibration, formation of supported lipid bilayers, exposure to PDDA-QDs, and AFM imaging. Supported lipid bilayers were formed following a previously published protocol[47] adapted to our solution conditions. Briefly, small unilamellar vesicles (0.0625 $mg \cdot mL^{-1}$) in the same solution were added to the dish to cover the bottom of the dish and the mica surface and heated for 1 h to 45 °C (above the transition temperature of all lipids used). Samples were allowed to cool to room temperature, and the liquid was exchanged with 12 mL (three 4 mL aliquots) of vesicle-free solution to remove loosely adhered vesicles, then with 12 mL (three 4 mL aliquots) of 0.150 M NaCl to remove excess calcium, and finally with 12 mL (three 4 mL aliquots) of 0.010 M NaCl solution to reduce ionic strength.

All images were collected in PeakForce Tapping™ mode using a Dimension Icon (Bruker) atomic force microscope. Gold-coated silicon nitride probes (Bruker, NPG) with a nominal force constant of 0.24 $N \cdot m^{-1}$ were employed. The gold coating reduced electrostatic interactions with the positively charged PDDA-QDs relative to more commonly used silicon nitride probes. Prior to imaging, the deflection sensitivity of the cantilever in air was determined using a fused silica reference sample. The force constant was also calibrated in air using the thermal tune method and fitting the power spectral density plot to a Lorentzian function.[49] Imaging was conducted in 0.010 M NaCl buffered to pH 7.4 with 0.010 M HEPES. The deflection sensitivity of the tip in liquid was re-calibrated using the previously determined force constant.[50-51]

Following calibration, the AFM head was raised, the calibration sample was removed, the bilayer sample in the dish was then placed onto the vacuum line of the AFM stage, and magnets were placed on

three sides of the dish to prevent movement of the dish during imaging. The AFM head was replaced and slowly lowered until the drop of buffer on the tip reached the submerged sample.

Images were collected at room temperature (24.5 °C). Supported lipid bilayers sometimes contain ~4 nm deep holes, extending to the underlying mica substrate. All experiments reported here used high quality bilayers that contained no holes or other defects over at least three regions scanned microns away from one another. We placed a registration marker on the bottom of the glass-bottom dish to ensure that same region could be found using the optical microscope on the AFM and that the same defect-free region was examined before and after exposure to nanomaterials. To minimize the effect of the mica substrate and electrostatic attractive forces that could occur between the positively charged quantum dots and the negatively charged mica due to holes in the bilayer,[18, 21] any bilayers found to contain holes or defects prior to PDDA-QD exposure were discarded. At least three images were collected for at least three different samples for each bilayer type studied prior to introduction of PDDA-QDs.

To examine the time scale of structural changes induced by exposure to PDDA-QDs, we initiated imaging immediately after introducing 1 nM QD suspensions in 0.010 M NaCl buffered to pH 7.4 with 0.010 M HEPES to the bilayers. Initial images took ~8 min to optimize and collect, and subsequent images were collected every ~4-5 min. We acquired images of the same region for up to 1 h. We also conducted experiments designed to match the sequence of solution changes used for QCM-D studies. In these experiments suspensions of 1 nM QDs in 0.010 M NaCl buffered to pH 7.4 with 0.010 M HEPES were added to the supported lipid bilayer and allowed to interact for 20 min. After 20 min, bilayers were rinsed with 12 mL (three 4 mL aliquots) of nanoparticle-free solution to remove any loosely adhered QDs, and imaging was immediately conducted at various spots on the bilayers. Resulting images were similar to those observed in the images collected over time. Control experiments were conducted to

investigate any topographic changes resulting from exposure of bilayers to free PDDA polymer. These control experiments employed poly(diallyldimethylammonium chloride) (Sigma, molecular mass 200,000-350,000 Da, 25 $\mu g \cdot mL^{-1}$) in 0.010 M NaCl buffered to pH 7.4 with 0.010 M HEPES . Determination of free polymer concentration in these solutions of quantum dots is difficult; the concentration used here was based on the concentration of polymer used in the functionalization and is therefore an overestimate. We chose to overestimate the polymer concentration to increase confidence that any effects observed were due to the quantum dots rather than to polymer free in solution. Control experiments were also conducted in which background solution was added instead of PDDA-QDs and imaging was immediately began to ensure that no changes in bilayer structure were observed due to sample preparation or changes over time.

RESULTS AND DISCUSSION

Characterization of PDDA-QDs. The PDDA-QDs were positively charged and had an electrophoretic mobility of a $(+2.6 \pm 0.3) \times 10^8$ m^2 V^{-1} s^{-1} in 0.010 M NaCl buffered to pH 7.4 with 0.010 M HEPES, the solution used in investigating interaction with supported lipid bilayers. The hydrodynamic diameter of these particles in this solution was 17 ± 1 nm, suggesting the particles were slightly aggregated in solution. The diameter determined by TEM was 6.1 ± 1.2 nm (Figure S3).

Formation of Zwitterionic Lipid Bilayers on SiO_2. We constructed supported bilayers composed of DOPC or 60/20/20 mol% DOPC/SM/Chol on SiO_2-coated QCM-D sensor crystals. We chose to work with DOPC because phosphatidylcholine is a majority component in the outer leaflet of eukaryotic cytoplasmic membranes.[38] The cholesterol- and sphingomyelin-containing bilayers were used to probe the importance of phase-segregated domains in the interaction of PDDA-QDs with bilayers. Both DOPC and SM possess zwitterionic phosphatidylcholine headgroups. Phosphatidylcholine bilayers formed on a

SiO_2 surface carry net negative potentials.[16, 52-53] The high affinity of SM for Chol promotes dense packing and formation of L_o domains.[54-55]

Figure S1 shows example QCM-D frequency and dissipation traces for the formation of DOPC and 60/20/20 mol% DOPC/SM/Chol bilayers. The traces exhibit the characteristic minimum in frequency and maximum in dissipation corresponding to the attainment of a critical surface vesicle concentration at which point the vesicles fuse and rupture, releasing the water contained within them and spontaneously form supported lipid bilayers.[56] Table S1 presents the frequency and dissipation values obtained for the bilayers after rinsing with vesicle-free solution to remove adhering vesicles. The DOPC bilayers exhibited final frequency changes of 24.8 ± 0.3 Hz, which corresponds to a mass of 446 ± 5 ng·cm^{-2} as approximated with the Sauerbrey equation,[43] and dissipation changes of 0.2 (± 0.1) × 10^{-6} (Table S1). These values are consistent with previous reports of well-formed DOPC bilayers under similar solution conditions.[15, 45, 56] The 60/20/20 mol% DOPC/SM/Chol bilayers had a final frequency changes of 27.0 ± 0.5 Hz, which corresponds to masses of 486 ± 9 ng·cm^{-2} and dissipation changes of 0.4 (± 0.1) × 10^{-6} (Table S1). These values are consistent with those previously reported for supported lipid bilayers containing L_o domains.[15]

Interaction of PDDA-QDs with DOPC and L_o Domain-containing Bilayers as Probed by QCM-D. We characterized the interaction of quantum dots with supported lipid bilayers described above by monitoring changes in frequency and dissipation upon introduction of PDDA-QDs to the flow chamber. Figure 1a shows the QCM-D frequency change as a function of time as quantum dots interact with a DOPC bilayer. Table 1 summarizes the observed changes in frequency and energy dissipation. At the longest exposures indicated prior to rinsing ($\Delta f_{20\,\mathrm{min}}$), the QCM-D resonance frequency decreased by 22.8 ± 1.2 Hz, which corresponds to a Sauerbrey mass of 410 ± 22 ng·cm^{-2}. The large frequency decrease demonstrates attachment of the positively charged nanoparticles to the bilayer, consistent with

favorable electrostatic interactions. Figure 1b shows the corresponding shift in dissipation factor associated with PDDA-QD attachment. The maximum change in dissipation before initiation of the rinse step was 1.8 (± 0.1) × 10^{-6}. Upon rinse, a small increase in frequency (3.8 ± 0.7 Hz) and drop in dissipation (–0.8 (± 0.1) × 10^{-6}) were observed, corresponding to a slight reduction in both surface-associated mass and energy dissipation. We attribute these changes to removal of loosely adsorbed quantum dots. Interestingly, approximately 10 min after the rinse began, the frequency rises sharply and dissipation increases dramatically. Ultimately, the frequency and dissipation values reach constant values corresponding to a net increase in dissipation (1.5 (± 0.2) × 10^{-6}) and no net change in frequency relative to the values immediately prior to the commencement of rinsing.

We next investigated the interaction of PDDA-QDs with phase-segregated SLBs using 60/20/20 mol% DOPC/SM/Chol bilayers. Figure 1c,d shows frequency and dissipation traces for the interaction of PDDA-QDs with a 60/20/20 mol% DOPC/SM/Chol bilayer. The attachment of PDDA-QDs to these phase-segregated bilayers produced maximum changes in frequency and dissipation ($\Delta f_{20\,\mathrm{min}}$ and $\Delta D_{20\,\mathrm{min}}$) of –18.2 ± 0.8 Hz (corresponding to a Sauerbrey mass of 328 ± 14 ng·cm^{-2}) and 1.3 (± 0.1) × 10^{-6} (Table 1). Figure 1c, d shows that upon rinsing, a small increase in frequency (2.2 ± 0.2 Hz) and decrease in dissipation (–0.6 (± 0.1) × 10^{-6}) were produced, followed closely by a sharp increase in dissipation and drop in frequency until plateau values are reached, similar to that observed for pure DOPC. The net effect of rinsing is an average increase in dissipation (2.0 (± 0.2) × 10^{-6}) and no mass change compared to the maximum values prior to rinse.

The extent of attachment to the DOPC and phase-segregated bilayers did not differ (p = 0.063 and 0.900, respectively, for $\Delta f_{20\,\mathrm{min}}$ and $\Delta D_{20\,\mathrm{min}}$), similar to a prior study[15] comparing the interaction of gold nanoparticles (AuNPs) functionalized with cationic mercaptopropylamine ($MPNH_2$) with the same bilayers under the same solution conditions as used here. In that study, the presence of phase-

segregated domains promoted attachment of $MPNH_2$-AuNPs at 0.1 M NaCl, an ionic strength higher than we employed in the present study. The results from our study differ from that on $MPNH_2$-AuNP in one important way: the changes in frequency and dissipation observed during rinsing in the present study did not occur in the study employing $MPNH_2$-AuNPs. This difference is presumably due primarily to the cationic molecules used to coat the nanoparticle surfaces. The nanoparticles used in the previous study were functionalized with short molecular ligands terminating in a primary amine.[15] In the present study, the QD were wrapped with PDDA polymer (average molecular mass of 200,000 Da) which has cyclic quaternary amine pendant groups.

To determine whether changes in frequency and energy dissipation observed during rinsing for the systems containing PDDA-QDs required the presence of a phospholipid bilayer, we conducted analogous experiments using SiO_2-coated QCM-D sensors lacking supported lipid bilayers. Figure S2 shows an example QCM-D trace from such a control experiment and demonstrates the attachment of PDDA-QDs to the SiO_2 substrate followed by stabilization of the frequency and dissipation values (Table 1). Rinsing the PDDA-QDs adhered to the silica substrate was not accompanied by the shifts in frequency (Figure S2a) or dissipation (Figure S2b) observed for these particles on DOPC bilayers. This result suggests that the presence of the bilayer is necessary for the frequency and dissipation changes observed upon rinsing attached PDDA-QDs (Figure 1a,b).

We hypothesize that the changes in frequency and dissipation occurring after removal of PDDA-QDs from the overlying solution during rinsing correspond to restructuring of the bilayer-QD system. We tested this hypothesis in the AFM experiments described below. We note that a previous study on the formation of negatively charged SLBs on QCM-D sensor surfaces reported similar trends in frequency and dissipation and attributed them to the restructuring of adsorbed phospholipids on the silica surface.[44]

Interaction with PDDA-QDs Induces Structural Changes to DOPC Bilayers. The results of the QCM-D experiments described above suggested that interaction of PDDA-QDs with both DOPC and 60/20/20 mol% DOPC/SM/Chol bilayers led to structural rearrangements. We monitored the interaction of the PDDA-QDs with both bilayer types using time-resolved AFM. Figure 2 (and the movie found in the Supporting Information) shows a time-lapse sequence for PDDA-QDs interacting with a DOPC bilayer. Prior to introduction of PDDA-QDs (Fig. 2a), the supported lipid bilayer had a uniformly smooth surface with RMS height variations < 110 pm, consistent with the DOPC bilayer following the topography of the underlying mica substrate. This uniformity is consistent with the fact that prior studies[15] have shown that under conditions similar to those of this experiment, DOPC is present in an entirely liquid-disordered phase. To confirm that the DOPC bilayer was present we conducted force-breakthrough curves (Figure S4) and observed that the layers exhibited a rupture event characteristic of SLBs. The breakthrough force observed for DOPC bilayers was ~3 nN and the discontinuity was ~4-5 nm in length corresponding to the height of the bilayer. These values were consistent with previous reports for DOPC SLBs[57] with exact values being dependent on the environmental conditions of the particular study (i.e., pH, temperature, rate of indentation).[58] After this confirmation we added quantum dots and immediately began imaging.

Figure 2b shows that the QDs caused structural changes immediately upon interaction with the DOPC bilayer. Starting with the first time point imaged after exposure of the bilayer to PDDA-QDs (at t = 8 min), the AFM data showed small regions 1.1 ± 0.2 nm in height, some of which contained taller features with heights of 8.6 ± 2.3 nm (Figure 3a, Table 2). We refer to the former as “microdomains” to distinguish them from the phase-segregated domains. The taller features appeared solely within the microdomains. The height of the taller features is consistent with the nanoparticle diameter determined from TEM images (6.1 ± 1.2 nm, Figure S3). In a control experiment we examined the impact of 25

μg·mL^{-1}PDDA polymer on bilayer structure in the absence of QDs (Figure 3b). This PDDA concentration is an overestimation of free polymer in solution and was based on the concentration of polymer used in the functionalization according to the manufacturer. We observed the formation of ~1 nm tall microdomains that lacked the taller features present in the some of the microdomains induced in DOPC bilayers exposed to PDDA-QDs. The ~1 nm high features are induced by interaction of the bilayer with PDDA or PDDA-QDs as the structure of the DOPC bilayer did not change over time after addition of PDDA-QD-free buffer (Figure S5a,b). We therefore conclude that the microdomains observed in Fig. 3b arise only after the bilayers are exposed to the PDDA polymer or the PDDA-QDs and that the tallest features likely correspond to PDDA-QDs. Similar structures have been reported previously, where the interaction of amphiphilic peptides with a DOPC bilayer produced locally high regions (~10 nm relative to the underlying DOPC bilayer) formed within microdomains (~1.4 nm taller than the underlying bilayer).[59] The authors of that study hypothesized that the tallest features were either large aggregates of peptides or partially solubilized/"budding" regions of the bilayer.[59] While we hypothesize in our study that the tallest features are quantum dots, we cannot rule out that the PDDA-QDs caused budding regions of the bilayers, whereas the polymer alone did not.

Exposure of bilayers to either PDDA-QDs or PDDA resulted in microdomain formation. We hypothesize that the microdomains arise from the interaction with the PDDA polymer – either wrapping the QDs or free in solution. The high local density of PDDA on the QDs and the comparatively large size of PDDA-QDs appears to lead to more pronounced structural perturbations relative to the polymer alone. Previous research on amine-terminated poly(amidoamine) dendrimers has shown that the degree of disruption to liquid crystalline supported phospholipid bilayers increases with dendritic generation and therefore dendrimer size.[60] The polymer alone induces formation of microdomains occupying 2.0 ± 1.9% of the total area over ~30 min, whereas exposure to PDDA-QDs resulted in a fractional coverage of 23.0

± 2.2% microdomains over this same time frame. Initial attachment likely occurs due to favorable electrostatic attraction between the positively charged quaternary amine pendant groups of the PDDA and the negative surface potential of the bilayer as has been reported previously with primary amines.[16, 53] Following initial attachment, we hypothesize that the hydrophobic backbone of the polymer likely extends into the hydrophobic core of the bilayer. The resulting mechanical stresses induce a height change in the surrounding bilayer. Such a height change can arise from changes in the tilt angle of the lipids with respect to the surface normal. The observed height change (1.1 ± 0.2 nm) is also consistent with the quantum dots inducing an increase in lipid ordering, due to more efficient packing of the hydrophobic tail groups, within the membrane.[61] However, an increase in lipid ordering and packing would be expected to lead to the formation of holes or a decrease in bilayer coverage,[59] neither of which are observed in Fig. 2. In Fig. 2b-h, the data show that over time more microdomains form, consistent with penetration of more particles into the bilayer over time. The formation of more microdomains over time is also consistent with the decrease in frequency and increase in dissipation observed by QCM-D. More quantum dots may penetrate the bilayer over time causing an increase in mass at the surface and a more dissipative final structure.

Interaction of PDDA-QDs with Phase-segregated Bilayers Cause L_o domains to Disappear. We next used *in situ* AFM imaging to examine the interaction of the quantum dots with a 60/20/20 mol% DOPC/SM/Chol bilayer over time. Figure 4a shows that this bilayer composition forms phase-segregated L_o domains, strongly enriched in sphingomyelin and cholesterol, that are ~1 nm higher in height than the L_d phase containing predominantly DOPC. This finding is consistent with previous work showing that cholesterol induces ordering of the unsaturated acyl chains of sphingomyelin, making the L_o regions ~1 nm taller than the L_d regions.[15, 61] The shape and lateral sizes of the L_o domains are also consistent with previous reports of similar bilayers on mica substrates.[48] Commencing with the first time point collected

after addition of the QDs, structural changes occurred similar to those observed with pure DOPC bilayers. Figure 4b shows the formation of microdomains in the L_d phases of the bilayer, encompassing taller features, consistent with our observations on liquid crystalline DOPC bilayers. We further found that the restructured lipids around the quantum dots were slightly taller (1.8 ± 0.2 nm, $p < 0.001$) than analogous structures in the DOPC bilayer (Figure 5b, Table 2). This increased height relative to the surrounding L_d phase is consistent with the positive amine groups of the PDDA-QDs binding to the phosphocholine headgroup of the lipid bilayers and the resulting mechanical stresses inducing a height change in the surrounding bilayer, much like our observations in the case of PDDA-QDs interacting with the DOPC bilayer. The larger thickness of the microdomains in phase-segregated SLBs relative to those formed in pure DOPC may be due to the presence of cholesterol in the L_d domains of the phase-segregated bilayers. A previous study showed that the presence of 30% cholesterol in a POPC bilayer increased its height by ~0.4 nm.[62] Therefore, the presence of cholesterol in the membranes used in our work, may account for the increase in height of the microdomains as compared to pure DOPC.

Upon addition of the QDs, the liquid-ordered domains of the DOPC/SM/Chol bilayer decrease in size and ultimately disappear within 15 min as clearly shown in Fig. 4d and 4e. Control experiments scanning the bilayer over the same length of time without exposure to PDDA-QDs showed no formation of microdomains or bright regions over the length scales of these studies (Figure S5c,d). Figure S5c, d shows that small L_o domains (< 0.06 μm^2) disappear over time without the addition of PDDA-QDs; however, Figure S6 shows that the addition of PDDA-QDs to the same bilayer in Figure S5 results in the complete disappearance of the phase-segregated domains within 20 min. This confirms that diffusion of the phase-segregated domains within the bilayer alone cannot account for the observed disappearance of the domains and that this effect is due to interaction with the PDDA-QDs. Figure S7 shows time-lapse images of free PDDA polymer (molecular mass 200,000 – 350,000, 25 $\mu g \cdot mL^{-1}$) interacting with a

60/20/20 mol% DOPC/SM/Chol bilayer. The interaction of free polymer with the bilayer also resulted in a decrease in the number and size of domain structures, but the effects of the free polymer were much less pronounced (domains still visible after 30 min of interaction) than those of the PDDA-QDs.

Prior studies of phase segregation in two-dimensional bilayer systems have highlighted the delicate balances of free energies involved.[63-64] In cases where the driving forces for phase segregation are small, subtle changes in composition may be sufficient to significantly alter the thermodynamic driving forces and thereby induce mixing.[63, 65-66] The destabilization of liquid-ordered domains has recently been reported for membrane proteins interacting with a model membrane containing L_o domains.[65] The lateral steric pressure, or energy per unit area, caused by protein-protein crowding on the surface of the membranes exceeded the approximate enthalpy of membrane mixing between the L_o and L_d phases, which resulted in the collapse of L_o domains.[65] Our results with amphiphilic positively charged quantum dots suggest similar phenomena are possible for nanomaterials. The increase in energy per area due to collisions between the bulky nanomaterials on the surface of the membrane may be enough to exceed the free energy of membrane mixing between the L_o and L_d phases, thus resulting in the destabilization of the L_o domains.

Overall, we propose that the forces between PDDA-QDs and SLBs (both DOPC and 60/20/20 mol% DOPC/SM/Chol) are driven by electrostatic attraction and the hydrophobic effect. We hypothesize that the initial interaction occurs between the positive charge on the quaternary amine and the negatively charged phosphate group of the phopholipids.[16, 53] Following this initial "anchoring," the hydrophobic backbone of the polymer inserts into the hydrophobic akyl chains of the lipid bilayer and causes restructuring around this site of contact. The QDs can then penetrate through the membrane or remain on top of the surface. Previous molecular dynamics[67-68] and experimental[69] studies have shown that hydrophobic ligands are able to anchor within the membrane. In the presence of L_o domains, the

additional energy per area induced by the addition of the PDDA-QDs to these systems, exceeds the enthalpy of membrane mixing and results in the mixing of the L_o and L_d phases. While this phenomenon has been shown previously following interactions with proteins[65] and polymers[66] in similar systems, we believe this to be the first evidence of positively charged quantum dots inducing the collapse of L_o domains.

SUMMARY AND CONCLUSIONS

Our results show that PDDA-QDs induce complex structural rearrangements of supported lipid bilayers consisting of 100% DOPC or 60/20/20 mol% DOPC/SM/Chol. The use of complementary, *in situ* analytical methods provided unprecedented insights into these structural changes. Namely, QCM-D shows that the interaction of QDs with the lipid bilayers induces structural rearrangements of the bilayers. Real-time *in situ* AFM imaging shows the formation of microdomains with higher features in the center of some microdomains that are consistent with quantum dots attached to the bilayer. Interestingly, the interaction of the positively charged amphiphilic quantum dots led to selective shrinkage of the liquid-ordered domains, with complete disappearance occurring after ~15 min of interaction. We hypothesize that the positive charge on the PDDA polymer interacts favorably with the negatively charged bilayers. Following this favorable interaction, the hydrophobic backbone of the polymer ligand can insert into the hydrophobic akyl chains of the bilayer and cause restructuring around this point of contact. Ultimately, when the additional energy per area caused by polymer-polymer, nanoparticle-nanoparticle, and/or nanoparticle-polymer collisions at the membrane surface exceeds the free energy of membrane mixing, the collapse of L_o domains was observed.

The present study represents an initial demonstration of the complex interactions that can occur between quantum dots wrapped with a positively charged, amphiphilic polymer, and supported lipid

bilayers. While more studies are necessary to generalize these results, other studies with amphiphilic and positively charged, hydrophobic ligands have shown similar features[59] and similar mechanisms of interaction were proposed.[68] Thus, we expect the results presented here will be most transferable to nanomaterials with positively charged hydrophobic or amphiphilic ligands.

ASSOCIATED CONTENT

Supporting Information. The Supporting Information is available free of charge on the ACS Publications website.

Frequency and dissipation QCM-D traces for DOPC and 60/20/20 mol% DOPC/SM/Chol bilayer formation and interaction with PDDA-QDs; Summary of frequency and dissipation shifts observed for DOPC and 60/20/20 mol% DOPC/SM/Chol bilayer formation; Changes in frequency and dissipation as a function of time as PDDA-QDs interact with the underlying SiO_2 substrate; TEM of the quantum dots; representative F_B curve on DOPC; time-lapse AFM of DOPC and 60/20/20 mol% DOPC/SM/Chol in the absence of PDDA-QDs; additional time-lapse AFM of PDDA-QDs interacting with a 60/20/20 mol% DOPC/SM/Chol bilayer; time lapse AFM of 60/20/20 mol% DOPC/SM/Chol exposed to 25 $\mu g \cdot mL^{-1}$PDDA polymer.

AUTHOR INFORMATION

Corresponding Author

*Phone: 608-262-6371; e-mail: rjhamers@wisc.edu.

*Phone: 608-263-4971; e-mail: joelpedersen@wisc.edu.

ORCID ID

Joseph T. Buchman: 0000-0001-5827-8513

Robert J. Hamers: 0000-0003-3821-9625

Christy L. Haynes: 0000-0002-5420-5867

Arielle C. Mensch: 0000-0002-4063-5882

Joel A. Pedersen: 0000-0002-3918-1860

Present Address

⊥ Environmental Molecular Sciences Laboratory, Pacific Northwest National Laboratory, Richland, WA 99354 United States.

Notes

The authors declare no competing financial interest.

ACKNOWLEDGMENTS

This work was supported by the National Science Foundation under the Center for Sustainable Nanotechnology, CHE-1503408. The CSN is part of the Centers for Chemical Innovation Program. J.T.B. was supported by the National Science Foundation Graduate Research Fellowship under Grant No. 00039202.

REFERENCES

1. Nel, A.; Xia, T.; Mädler, L.; Li, N., Toxic potential of materials at the nanolevel. *Science,* **2006,** *311*, 622-627.

2. Christian, P.; Von der Kammer, F.; Baalousha, M.; Hofmann, T., Nanoparticles: Structure, properties, preparation and behaviour in environmental media. *Ecotoxicology,* **2008,** *17*, 326-43.

3. Maurer-Jones, M. A.; Gunsolus, I. L.; Murphy, C. J.; Haynes, C. L., Toxicity of engineered nanoparticles in the environment. *Anal. Chem.,* **2013,** *85*, 3036-49.

4. Hamers, R. J., Nanomaterials and global sustainability. *Acc. Chem. Res.,* **2017,** *50*, 633-637.

5. Louie, S. M.; Dale, A. L.; Casman, E. A.; Lowry, G. V., Challenges facing the environmental nanotechnology research enterprise. In *Engineered nanoparticles and the environment: Biophysicochemical processes and toxicity*, Xing, B.; Vectis, C. D.; Senesi, N., Eds. 2016; Vol. 4, pp 3-19.

6. Felix, L. C.; Ortega, V. A.; Goss, G. G., Cellular uptake and intracellular localization of poly (acrylic acid) nanoparticles in a rainbow trout (*Oncorhynchus mykiss*) gill epithelial cell line, RTgill-W1. *Aquat. Toxicol.,* **2017,** *192*, 58-68.

7. Ding, B.; Tian, Y.; Pan, Y.; Shan, Y.; Cai, M.; Xu, H.; Sun, Y.; Wang, H., Recording the dynamic endocytosis of single gold nanoparticles by AFM-based force tracing. *Nanoscale,* **2015,** *7*, 7545-9.

8. Chen, J.; Hessler, J. A.; Putchakayala, K.; Panama, B. K.; Khan, D. P.; Hong, S.; Mullen, D. G.; DiMaggio, S. C.; Som, A.; Tew, G. N.; Lopatin, A. N.; James R. Baker, J.; Holl, M. M. B.; Orr, B. G., Cationic nanoparticles induce nanoscale disruption in living cell plasma membranes. *J. Phys. Chem. B,* **2009,** *113*, 11179-11185.

9. Leroueil, P. R.; Hong, S.; Mecke, A.; Jr., J. R. B.; Orr, B. G.; Holl, M. M. B., Nanoparticle interaction with biological membranes: Does nanotechnology present a Janus face? *Acc. Chem. Res.,* **2007,** *40*, 335-342.

10. Zhu, W.; von dem Bussche, A.; Yi, X.; Qiu, Y.; Wang, Z.; Weston, P.; Hurt, R. H.; Kane, A. B.; Gao, H., Nanomechanical mechanism for lipid bilayer damage induced by carbon nanotubes confined in intracellular vesicles. *Proc. Natl. Acad. Sci. U.S.A.,* **2016,** *113*, 12374-12379.

11. Kim, M. S.; Louis, K. M.; Pedersen, J. A.; Hamers, R. J.; Peterson, R. E.; Heideman, W., Using citrate-functionalized TiO_2 nanoparticles to study the effect of particle size on zebrafish embryo toxicity. *Analyst,* **2014,** *139*, 964-72.

12. Hang, M. N.; Gunsolus, I. L.; Wayland, H.; Melby, E. S.; Mensch, A. C.; Hurley, K. R.; Pedersen, J. A.; Haynes, C. L.; Hamers, R. J., Impact of nanoscale lithium nickel manganese cobalt oxide (NMC) on the bacterium *Shewanella oneidensis MR-1*. *Chem. Mater.,* **2016,** *28*, 1092-1100.

13. Lesniak, A.; Salvati, A.; Santos-Martinez, M. J.; Radomski, M. W.; Dawson, K. A.; Åberg, C., Nanoparticle adhesion to the cell membrane and its effect on nanoparticle uptake efficiency. *J. Am. Chem. Soc.,* **2013,** *135*, 1438-44.

14. Goodman, C. M.; McCusker, C. D.; Yilmaz, T.; Rotello, V. M., Toxicity of gold nanoparticles functionalized with cationic and anionic side chains. *Bioconjugate Chem.,* **2004,** *15*, 897-900.

15. Melby, E. S.; Mensch, A. C.; Lohse, S. E.; Hu, D.; Orr, G.; Murphy, C. J.; Hamers, R. J.; Pedersen, J. A., Formation of supported lipid bilayers containing phase-segregated domains and their interaction with gold nanoparticles. *Environ. Sci.: Nano,* **2016,** *3*, 45-55.

16. Troiano, J. M.; Olenick, L. L.; Kuech, T. R.; Melby, E. S.; Hu, D.; Lohse, S. E.; Mensch, A. C.; Dogangun, M.; Vartanian, A. M.; Torelli, M. D.; Ehimiaghe, E.; Walter, S. R.; Fu, L.; Anderton, C. R.; Zhu, Z.; Wang, H.; Orr, G.; Murphy, C. J.; Hamers, R. J.; Pedersen, J. A.; Geiger, F. M., Direct probes of 4 nm diameter gold nanoparticles interacting with supported lipid bilayers. *J. Phys. Chem. C,* **2015,** *119*, 534-546.

17. Chen, K. L.; Bothun, G. D., Nanoparticles meet cell membranes: Probing nonspecific interactions using model membranes. *Environ. Sci. Technol.,* **2014,** *48*, 873-80.

18. Leroueil, P. R.; Berry, S. A.; Duthie, K.; Han, G.; Rotello, V. M.; McNerny, D. Q.; Jr., J. R. B.; Orr, B. G.; Holl, M. M. B., Wide varieties of cationic nanoparticles induce defects in supported lipid bilayers. *Nano Letters,* **2008,** *8*, 420-424.

19. Jacobson, K. H.; Gunsolus, I. L.; Kuech, T. R.; Troiano, J. M.; Melby, E. S.; Lohse, S. E.; Hu, D.; Chrisler, W. B.; Murphy, C. J.; Orr, G.; Geiger, F. M.; Haynes, C. L.; Pedersen, J. A., Lipopolysaccharide density and structure govern the extent and distance of nanoparticle interaction with actual and model bacterial outer membranes. *Environ. Sci. Technol.,* **2015,** *49*, 10642-50.

20. Melby, E. S.; Allen, C. R.; Foreman-Ortiz, I. U.; Caudill, E. R.; Kuech, T. R.; Vartanian, A. M.; Zhang, X.; Murphy, C. J.; Hernandez, R. T.; Pedersen, J. A., Peripheral membrane proteins dramatically alter nanoparticle interaction at lipid bilayer interfaces. *Langmuir*, (in review).

21. Hong, S.; Bielinska, A. U.; Mecke, A.; Keszler, B.; Beals, J. L.; Shi, X.; Balogh, L.; Orr, B. G.; James R. Baker, J.; Holl, M. M. B., Interaction of poly(amidoamine) dendrimers with supported lipid bilayers and cells: Hole formation and the relation to transport. *Bioconjugate Chem.,* **2004,** *15*, 774-782.

22. Lee, K.; Zhang, L.; Yi, Y.; Wang, X.; Yu, Y., Rupture of lipid membranes induced by amphiphilic Janus nanoparticles. *ACS Nano,* **2018,** *12*, 3646-3657.

23. Jing, B.; Abot, R. C.; Zhu, Y., Semihydrophobic nanoparticle-induced disruption of supported lipid bilayers: Specific ion effect. *J. Phys. Chem. B,* **2014,** *118*, 13175-82.

24. Bramkamp, M.; Lopez, D., Exploring the existence of lipid rafts in bacteria. *Microbiol. Mol. Biol. Rev.,* **2015,** *79*, 81-100.

25. Sezgin, E.; Levental, I.; Mayor, S.; Eggeling, C., The mystery of membrane organization: Composition, regulation and roles of lipid rafts. *Nat. Rev. Mol. Cell Biol.,* **2017,** *18*, 361-374.

26. Simons, K.; Ikonen, E., Functional rafts in cell membranes. *Nature,* **1997,** *387*, 569-572.

27. Lind, T. K.; Zielińska, P.; Wacklin, H. P.; Urbańczyk-Lipkowska, Z.; Cárdenas, M., Continuous flow atomic force microscopy imaging reveals fluidity and time-dependent interactions of antimicrobial dendrimer with model lipid membranes. *ACS Nano,* **2014,** *8*, 396-408.

28. Chelladurai, R.; Debnath, K.; Jana, N. R.; Basu, J. K., Nanoscale heterogeneities drive enhanced binding and anomalous diffusion of nanoparticles in model biomembranes. *Langmuir,* **2018,** *34*, 1691-1699.

29. Mecke, A.; Lee, D.-K.; Ramamoorthy, A.; Orr, B. G.; Holl, M. M. B., Synthetic and natural polycationic polymer nanoparticles interact selectively with fluid-phase domains of DMPC lipid bilayers. *Langmuir,* **2005,** *21*, 8588-8590.

30. Erickson, B.; DiMaggio, S. C.; Mullen, D. G.; Kelly, C. V.; Leroueil, P. R.; Berry, S. A.; Baker, J. R., Jr.; Orr, B. G.; Banaszak Holl, M. M., Interactions of poly(amidoamine) dendrimers with Survanta lung surfactant: The importance of lipid domains. *Langmuir,* **2008,** *24*, 11003-8.

31. Chakraborty, A.; Mucci, N. J.; Tan, M. L.; Steckley, A.; Zhang, T.; Forrest, M. L.; Dhar, P., Phospholipid composition modulates carbon nanodiamond-induced alterations in phospholipid domain formation. *Langmuir,* **2015,** *31*, 5093-104.

32. Moghadam, B. Y.; Hou, W. C.; Corredor, C.; Westerhoff, P.; Posner, J. D., Role of nanoparticle surface functionality in the disruption of model cell membranes. *Langmuir,* **2012,** *28*, 16318-26.

33. Mensch, A. C.; Tapia Hernandez, R.; Kuether, J. E.; Torelli, M. D.; Feng, Z. V.; Hamers, R. J.; Pedersen, J. A., Natural organic matter concentration impacts the interaction of functionalized diamond nanoparticles with model and actual bacterial membranes. *Environ. Sci. Technol.,* **2017,** *51*, 11075-11084.

34. Martynenko, I. V.; Litvin, A. P.; Purcell-Milton, F.; Baranov, A. V.; Fedorov, A. V.; Gun'ko, Y. K., Application of semiconductor quantum dots in bioimaging and biosensing. *J. Mater. Chem. B,* **2017,** *5*, 6701-6727.

35. Rühle, S.; Shalom, M.; Zaban, A., Quantum-dot-sensitized solar cells. *ChemPhysChem,* **2010,** *11*, 2290-304.

36. Hardman, R., A toxicologic review of quantum dots: Toxicity depends on physicochemical and environmental factors. *Environ. Health Perspect.,* **2006,** *114*, 165-172.

37. King-Heiden, T. C.; Wiecinski, P. N.; Mangham, A. N.; Metz, K. M.; Nesbit, D.; Pedersen, J. A.; Hamers, R. J.; Heideman, W.; Peterson, R. E., Quantum dot nanotoxicity assessment using the zebrafish embryo. *Environ. Sci. Technol.,* **2009,** *43*, 1605-1611.

38. Brown, D. A.; London, E., Functions of lipid rafts in biological membranes. *Annu. Rev. Cell Dev. Biol.,* **1998,** *14*, 111-136.

39. Malvern Instruments, *Intensity-volume-number: What size is correct?*; Technical Note MRK1357-01; Malvern Instruments: Malvern, United Kingdom; 2009.

40. Barton, P. G.; Gunstone, F. D., Hydrocarbon chain packing and molecular motion in phospholipid bilayers formed from unsaturated lecithins. Synthesis and properties of sixteen positional isomers of 1,2-dioctadecenoyl-sn-glycero-3-phosphorylcholine. *J. Biol. Chem.,* **1975,** *250*, 4470-4476.

41. Estep, T. N.; Mountcastle, D. B.; Barenholz, Y.; Biltonen, R. L.; Thompson, T. E., Thermal behavior of synthetic sphingomyelin-cholesterol dispersions. *Biochem.,* **1979,** *18*, 2112-2117.

42. Reviakine, I.; Johannsmann, D.; Richter, R. P., Hearing what you cannot see and visualizing what you hear: Interpreting quartz crystal microbalance data from solvated interfaces. *Anal. Chem.,* **2011,** *83*, 8838-48.

43. Sauerbrey, G., Verwendung von Schwingquarzen zur Wägung dünner Schichten und zur Mikrowägung. *Zeitschrift für Physik,* **1959,** *155*, 206-222.

44. Richter, R.; Mukhopadhyay, A.; Brisson, A., Pathways of lipid vesicle deposition on solid surfaces: A combined QCM-D and AFM study. *Biophys. J.,* **2003,** *85*, 3035-3047.

45. Keller, C. A.; Kasemo, B., Surface specific kinetics of lipid vesicle adsorption measured with a quartz crystal microbalance. *Biophys. J.,* **1998,** *75*, 1397-1402.

46. Richter, R. P.; Brisson, A. R., Following the formation of supported lipid bilayers on mica: A study combining AFM, QCM-D, and ellipsometry. *Biophys. J.,* **2005,** *88*, 3422-33.

47. Sullan, R. M.; Li, J. K.; Zou, S., Direct correlation of structures and nanomechanical properties of multicomponent lipid bilayers. *Langmuir,* **2009,** *25*, 7471-7.

48. Sullan, R. M.; Li, J. K.; Hao, C.; Walker, G. C.; Zou, S., Cholesterol-dependent nanomechanical stability of phase-segregated multicomponent lipid bilayers. *Biophys. J.,* **2010,** *99*, 507-16.

49. Hutter, J. L.; Bechhoefer, J., Calibration of atomic-force microscope tips. *Rev. Sci. Instrum.,* **1993,** *64*, 1868-1873.

50. Ohler, B., *Practical advice on determination of cantilever spring constants*; Veeco: 2007.

51. Butt, H. J.; Jaschke, M., Calculation of thermal noise in atomic force microscopy. *Nanotechnology,* **1995,** *6*, 1-7.

52. Zimmermann, R.; Küttner, D.; Renner, L.; Kaufmann, M.; Zitzmann, J.; Müller, M.; Werner, C., Charging and structure of zwitterionic supported bilayer lipid membranes studied by streaming current measurements, fluorescence microscopy, and attenuated total reflection Fourier transform infrared spectroscopy. *Biointerphases,* **2009,** *4*, 1-6.

53. Kuech, T. R. Biological interactions and environmental transformations of nanomaterials. Ph. D. Dissertation, University of Wisconsin-Madison, 2015.

54. Slotte, J. P., Biological functions of sphingomyelins. *Prog. Lipid Res.,* **2013,** *52*, 424-37.

55. Quinn, P. J., Structure of sphingomyelin bilayers and complexes with cholesterol forming membrane rafts. *Langmuir,* **2013,** *29*, 9447-56.

56. Cho, N. J.; Frank, C. W.; Kasemo, B.; Hook, F., Quartz crystal microbalance with dissipation monitoring of supported lipid bilayers on various substrates. *Nat Protoc,* **2010,** *5*, 1096-106.

57. Attwood, S. J.; Choi, Y.; Leonenko, Z., Preparation of DOPC and DPPC supported planar lipid bilayers for atomic force microscopy and atomic force spectroscopy. *Int. J. Mol. Sci.,* **2013,** *14*, 3514-39.

58. Alessandrini, A.; Seeger, H. M.; Di Cerbo, A.; Caramaschi, T.; Facci, P., What do we really measure in AFM punch-through experiments on supported lipid bilayers? *Soft Matter,* **2011,** *7*, 7054.

59. Rigby-Singleton, S. M.; Davies, M. C.; Harris, H.; O'Shea, P.; Allen, S., Visualizing the solubilization of supported lipid bilayers by an amphiphilic peptide. *Langmuir,* **2006,** *22*, 6273-6279.

60. Mecke, A.; Majoros, I. J.; Patri, A. K.; James R. Baker, J.; Holl, M. M. B.; Orr, B. G., Lipid bilayer disruption by polycationic polymers: The roles of size and chemical functional group. *Langmuir,* **2005,** *21*, 10348-10354.

61. Chiantia, S.; Kahya, N.; Ries, J.; Schwille, P., Effects of ceramide on liquid-ordered domains investigated by simultaneous AFM and FCS. *Biophys. J.,* **2006,** *90*, 4500-8.

62. Nezil, F. A.; Bloom, M., Combined influence of cholesterol and synthetic amphiphillic peptides upon bilayer thickness in model membranes. *Biophys. J.,* **1992,** *61*, 1176-1183.

63. Honerkamp-Smith, A. R.; Cicuta, P.; Collins, M. D.; Veatch, S. L.; den Nijs, M.; Schick, M.; Keller, S. L., Line tensions, correlation lengths, and critical exponents in lipid membranes near critical points. *Biophys. J.,* **2008,** *95*, 236-46.

64. Honerkamp-Smith, A. R.; Veatch, S. L.; Keller, S. L., An introduction to critical points for biophysicists; observations of compositional heterogeneity in lipid membranes. *Biochim. Biophys. Acta,* **2009,** *1788*, 53-63.

65. Scheve, C. S.; Gonzales, P. A.; Momin, N.; Stachowiak, J. C., Steric pressure between membrane-bound proteins opposes lipid phase separation. *J. Am. Chem. Soc.,* **2013,** *135*, 1185-8.

66. Imam, Z. I.; Kenyon, L. E.; Carrillo, A.; Espinoza, I.; Nagib, F.; Stachowiak, J. C., Steric pressure among membrane-bound polymers opposes lipid phase separation. *Langmuir,* **2016,** *32*, 3774-84.

67. Gkeka, P.; Angelikopoulos, P.; Sarkisov, L.; Cournia, Z., Membrane partitioning of anionic, ligand-coated nanoparticles is accompanied by ligand snorkeling, local disordering, and cholesterol depletion. *PLoS Comput. Biol.,* **2014,** *10*, e1003917.

68. Van Lehn, R. C.; Alexander-Katz, A., Pathway for insertion of amphiphilic nanoparticles into defect-free lipid bilayers from atomistic molecular dynamics simulations. *Soft Matter,* **2015,** *11*, 3165-75.

69. Smith, P. E. S.; Brender, J. R.; Dürr, U. H. N.; Xu, J.; Mullen, D. G.; Holl, M. M. B.; Ramamoorthy, A., Solid state NMR reveals the hydrophobic-core location of poly(amidoamine) dendrimers in biomembranes. *J. Am. Chem. Soc.,* **2010,** *132*, 8087-8097.

70. Grennan, A. K., Lipid rafts in plants. *Plant Physiol.,* **2007,** *143*, 1083-5.

71. Alvarez, F. J.; Douglas, L. M.; Konopka, J. B., Sterol-rich plasma membrane domains in fungi. *Eukaryot. Cell,* **2007,** *6*, 755-63.

Table 1. Summary of frequency shifts (Δf) and dissipation changes (ΔD) upon interaction between PDDA-QDs and the indicated supported lipid bilayer or silica surface as measured by quartz crystal microbalance with dissipation monitoring.[a]

Bilayer Type	$\Delta f_{20\ min}$ (Hz)	$\Delta D_{20\ min}$ ($\times 10^{-6}$)	Δf_{rinsed} (Hz)	ΔD_{rinsed} ($\times 10^{-6}$)
DOPC	–22.8 ± 1.2	1.8 ± 0.1	–21.7 ± 1.8	3.3 ± 0.3
DOPC/SM/Chol	–18.2 ± 0.8	1.3 ± 0.1	–18.7 ± 2.4	3.3 ± 0.2
SiO_2	–15.5 ± 0.4	0.6 ± 0.01	–15.5 ± 0.3	0.5 ± 0.04

[a] Attachment experiments were conducted in 0.010 M NaCl buffered to pH 7.4 with 0.010 M HEPES at 25 °C. All data are for the 3rd harmonic. Data for the frequency and dissipation shifts are after 20 min of attachment or for the final equilibrated values following rinse with buffer. Values are means ± standard deviations of at least triplicate experiments. Abbreviations: DOPC, 1,2-dioleoyl-*sn*-glycero-3-phosphocholine; SM, sphingomyelin; Chol, cholesterol.

Table 2. Line scan analysis of features observed by AFM.[a]

Bilayer Type	Microdomain Height[b] (nm)	Particle Height within Microdomains[b] (nm)
DOPC	1.1 ± 0.2 (*N* = 26)	8.6 ± 2.3 (*N* = 31)
DOPC/SM/Chol	1.8 ± 0.2 (*N* = 25)	7.7 ± 2.6 (*N* = 31)

[a] AFM experiments were conducted in 0.010 M NaCl buffered to pH 7.4 with 0.010 M HEPES at 24.5 °C. Values are averages and standard deviations of *N* line scans. Abbreviations: DOPC, 1,2-dioleoyl-*sn*-glycero-3-phosphocholine; SM, sphingomyelin; Chol, cholesterol.

[b] Referenced to underlying bilayer.

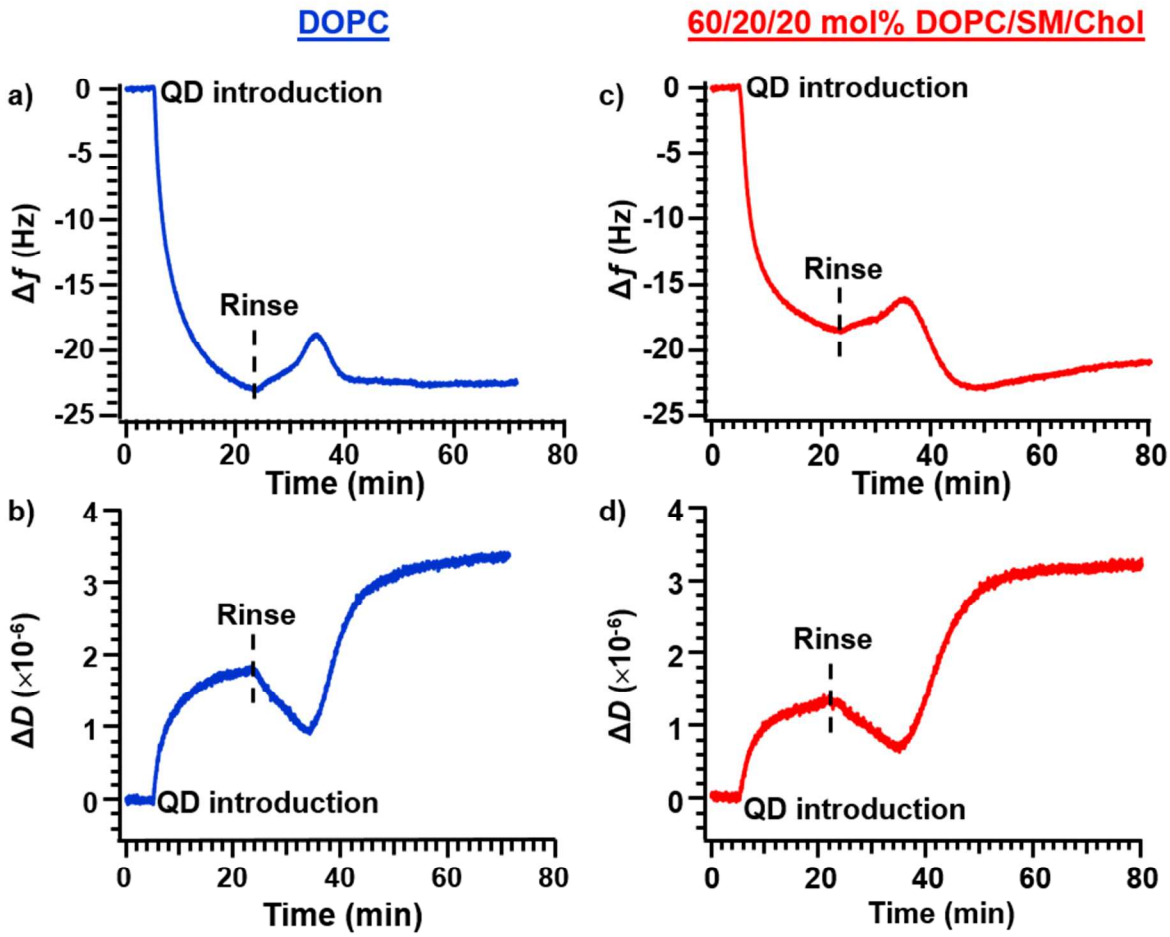

Figure 1. Representative changes in a, c) frequency and b, d) dissipation upon introduction of 1 nM PDDA-QDs to a a,b) DOPC or c,d) 60/20/20 mol% DOPC/SM/Chol bilayer in 0.01 M NaCl buffered to pH 7.4 with 0.01 M HEPES. The bilayer has already been formed and interaction between the QDs and the bilayer begins where noted. The dashed line represents the point where buffer without QDs reach the sensor surface and some mass loss and decrease in dissipation is initially observed. All data are for the 3rd harmonic.

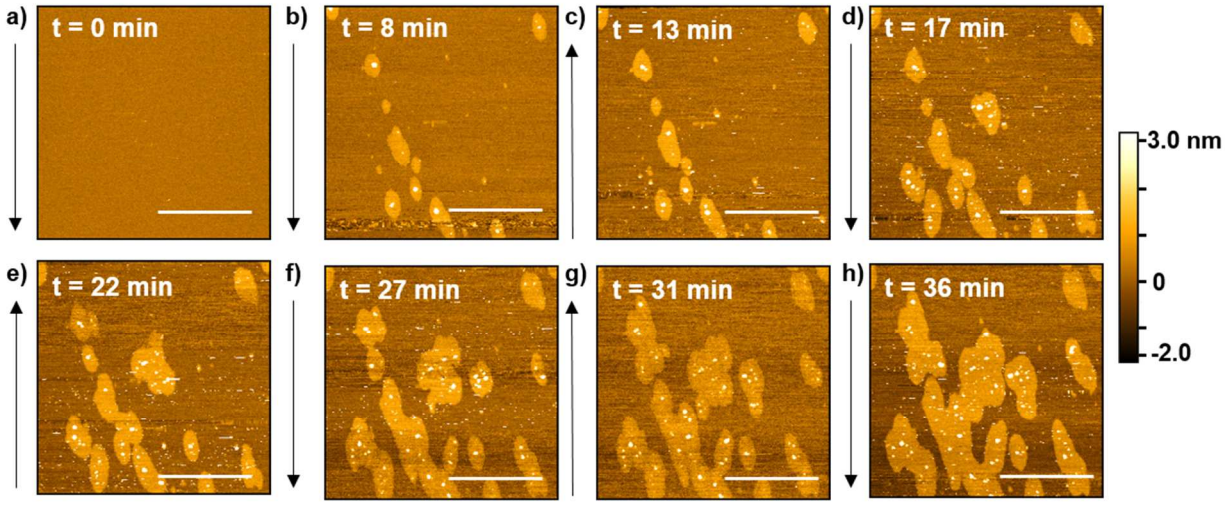

Figure 2. Time-lapse topographical AFM images showing the impact of PDDA-QDs on a DOPC bilayer immediately after injection of particles. a) DOPC bilayer prior to the introduction of PDDA-QDs, b-h) subsequent images taken after interaction with the PDDA-QDs. All images were collected in 0.01 M NaCl buffered to pH 7.4 with 0.01 M HEPES at 24.5 °C. Black arrows represent the scan direction for the given image. Scale bars on all images are 2 µm. Z-height color scale corresponds to all images. The time on each image indicates how much time the bilayer had been in contact with PDDA-QDs. Each image took between 4-6 min to capture depending on optimization of scan parameters. A video of this sequence can be found in the supporting information.

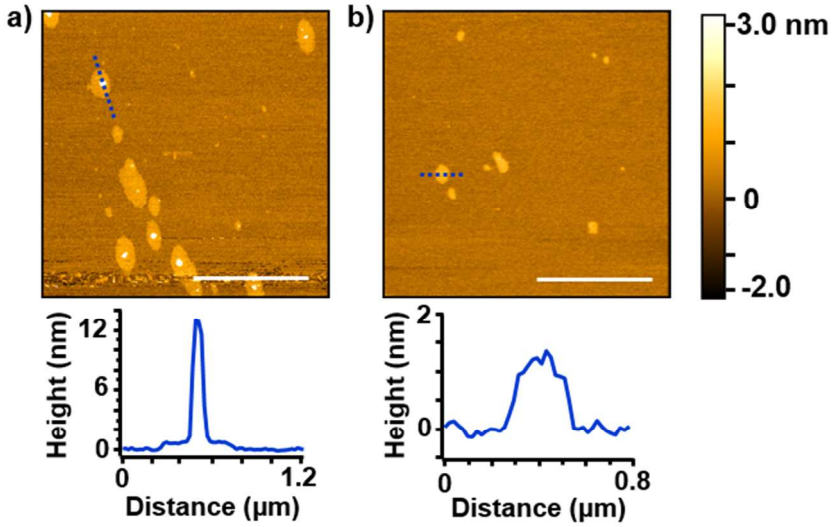

Figure 3. a) Line profile across the microdomains observed after interaction of PDDA-QDs with the DOPC bilayer from Figure 2a and b) PDDA polymer (molecular mass 200,000-350,000 Da, 0.0025 wt. %) interaction with a DOPC bilayer with corresponding line scan. All images were collected in 0.01 M NaCl buffered to pH 7.4 with 0.01 M HEPES at 24.5 °C. Line scans were taken across the dashed blue line in each image. Scale bars on all images are 2 μm. Z-height color scale corresponds to both images.

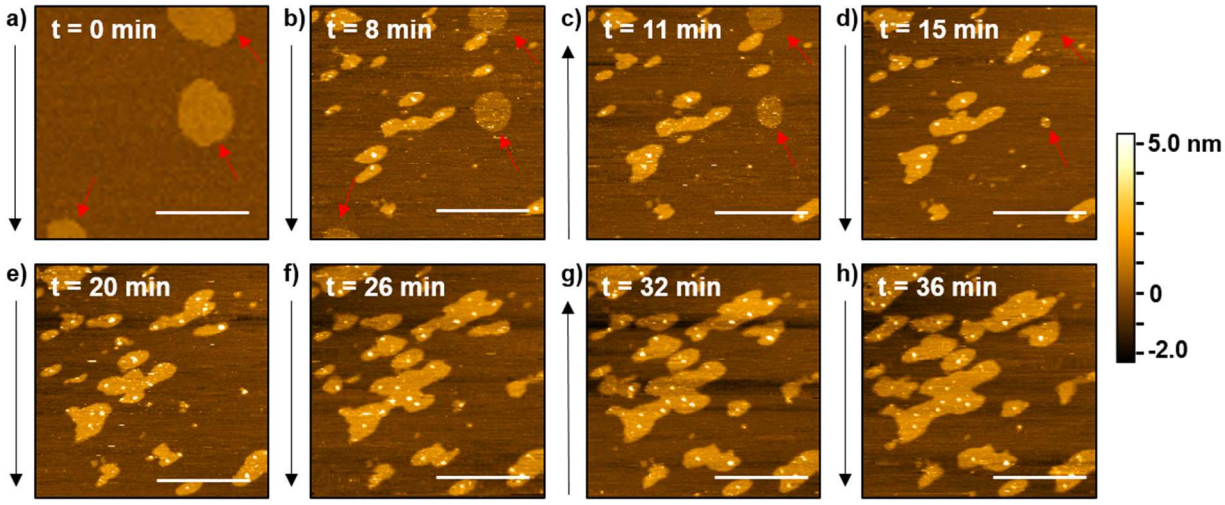

Figure 4. Time-lapse topographical AFM images showing the effect of PDDA-QDs on a bilayer initially containing phase-segregated domains. Bilayer composition was 60/20/20 mol% DOPC/SM/Chol. a) Bilayer prior to the introduction of PDDA-QDs, b-h) subsequent images taken after interaction with the PDDA-QDs. All images were collected in 0.01 M NaCl buffered to pH 7.4 with 0.01 M HEPES at 24.5 °C. Black arrows represent the scan direction for the given image. Scale bars on all images are 2 µm. The red arrows are intended to direct the reader's eye to the disappearance of the liquid-ordered domains. Z-height color scale corresponds to all images. The time on each image indicates how much time the bilayer had been in contact with PDDA-QDs. Each image took between 3-6 min to capture depending on optimization of scan parameters. A video of this sequence can be found in the supporting information.

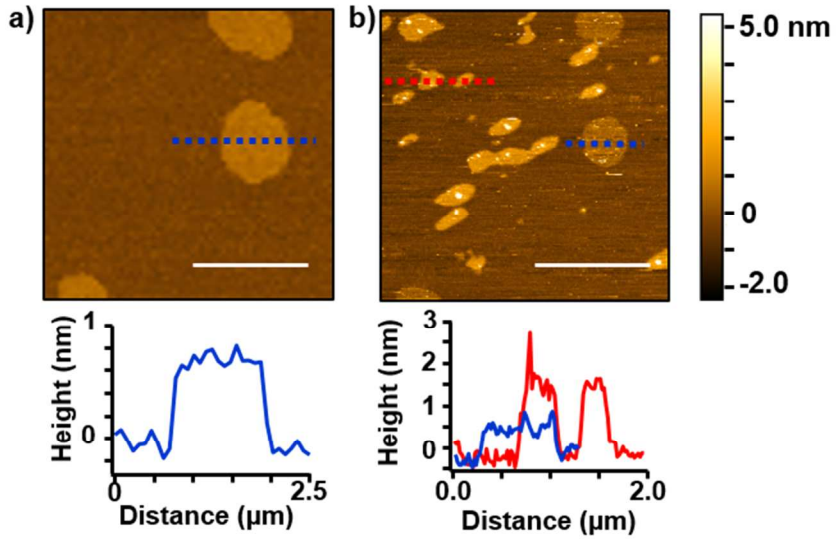

Figure 5. Representative line traces observed for height across features observed in a 60/20/20 mol% DOPC/SM/Chol bilayer (note: same bilayer as presented in Figure 4) a) prior to and b) after interaction with 1 nM PDDA-QDs. The blue trace traces in both images show the height over a liquid-ordered domain, whereas the red trace in b) shows the height across the microdomain structure induced by the PDDA-QDs. All images were collected in 0.01 M NaCl buffered to pH 7.4 with 0.01 M HEPES at 24.5 °C. Scale bars are 2 μm. Z-height color scale corresponds to both images.

TOC Image